Assessing the Load-Carrying Capacity of Composite Castellated Beams by Finite Element Method

Mohammad Sadeghi [1]; Ehsan Dehghani [2,*]; Mohammad Ali Fathali [3]

1. M.Sc. Student, Department of Civil Engineering, Faculty of Engineering, University of Qom, Qom, Iran
2. Associate Professor, Department of Civil Engineering, Faculty of Engineering, University of Qom, Qom, Iran
3. Assistant Professor, Faculty of Engineering, Mahallat Institute of Higher Education, Mahallat, Iran
* Corresponding author: dehghani@qom.ac.ir

ARTICLE INFO

ABSTRACT

The utilization of composite castellated beams in structures is common due to the increased bending strength and stiffness of the beam. However, the presence of openings in castellated beams reduces their shear strength. The increased bending strength allows these beams to be used over longer spans; however, the reduced shear strength makes shear force effects more pronounced in such beams. In this study, a comparative analysis of the behaviors of composite beams with castellated and solid-web has been conducted using finite element method. Nine composite castellated beams and nine solid-web composite beams, both with equal heights and cross-sectional areas, were modeled based on castellated configurations. The AISC Design Guide 31 (DG31) provides a method for calculating the ultimate bending capacity of composite castellated beams but neglects the contribution of the upper T-shaped section of the castellated beam. In this study, the focus is on innovatively comparing the load-carrying capacity of composite castellated beams with the AISC DG31 results, highlighting how finite element analysis reveals higher capacities than those predicted by DG31 by 17% to 31% across specimens. It is observed that the load-carrying capacity of castellated specimens is 2% to 5% lower than that of specimens with solid-webs. This difference may increase up to 22% with local failure in the web-post if the first openings of the beam are placed too close to the supports. Notably, the research demonstrates that the web openings in castellated beams have a minor effect on load-carrying capacity, suggesting that despite reduced shear strength, these openings do not significantly impact the overall capacity, particularly when placed thoughtfully in structural design.

How to cite this article:

1. Introduction

The utilization of castellated sections has become more prevalent with the advancement of welding techniques and their incorporation into the construction industry in the early 1950s, due to their enhanced flexural strength and material efficiency. The incorporation of castellated beams in composite floors, results in an increase in the flexural resistance and preventing the lateral-torsional buckling mode in the beam. When loads are applied, the web openings disrupt the distribution of internal stresses. The steel above and below the openings must transfer forces around the opening, inducing localized bending moments and shear stresses. This results in significant moments at the edges of the web openings, where the beam acts like a series of small, rigid frames similar to a vierendeel truss. At higher loads, plastic hinges can form at the corners of the web openings due to the high bending moments, particularly in the horizontal segments of the webs between the openings. This can lead to a failure mechanism if not properly designed or accounted for [1]. This mechanism is one of the primary modes of failure in composite castellated beams, requiring appropriate control measures to prevent its occurrence.

In the first studies on castellated beams, the maximum displacement was calculated using static analysis by modeling a castellated beam as an equivalent vierendeel truss [2]. Taking into account the flexural and shear stiffness of the equivalent vierendeel truss, has improved the accuracy of the calculated displacement [3,4]. Kerdal and Nethercot investigated the behavior of castellated beams using experimental research and reported various failure modes [5]. The results of this research showed that the vierendeel mechanism, flexure failure and web-post buckling are the most likely failure mechanisms in such beams.

Redwood and Cho conducted an investigation into the behavior of composite beams with openings in the web, utilizing experimental research methods [6]. This article reports and discusses the failure modes observed in such beams. The article also presents a design approach for mitigating the effects of interactions between bending moments and shear force on these openings. This is achieved through calculations of the bending moment and shear force at the opening locations. According to the results of this study, the bending capacity and shear strength of composite castellated beams increased by 22% and 55%, respectively, when compared to non-composite castellated beams.

Chung and Lawson proposed a design method based on Eurocode 4 [7] for designing composite beams with one or multiple large openings in the web [8]. The proposed design method has been validated through experimental research. Furthermore, based on the test results, optimal position for placing openings along the span have been established under various loads and support conditions. The results of research of composite beams with web openings have shown that in cases where the width of the opening is large, the vierendeel mechanism will be the primary failure mode.

Wang and Chung investigated composite beams with web openings in the presence of flexible shear connectors using finite element analysis [9]. The findings of this study showed that the assumed behavior of shear connectors has a significant impact on the accuracy of the performed analysis. Furthermore, a large pull-out force is observed in the shear connectors near the openings, which has not previously been reported. Previous studies have been interested in investigating the interaction of concrete and shear connectors in composite beams. The mechanical properties of the shear connector are among the important parameters in finite element analysis on composite beams. The results of the studies indicate that the load–slip behavior of shear connectors [10] and the effects of cracking in concrete [11] have a significant impact on the accuracy of the obtained displacement of the beam. When the shear connector is defined as a solid element in the finite element analysis, there is no requirement to specify the load-slip behavior, and the results are accurate [12].

Yang et al. investigated making an opening in the web near the beam-to-column connection as an attempt to ensure the formation of plastic hinges firstly in the beam [10]. Due to the possibility of brittle failure at the beam-to-column connection in moment-resisting frames, implementing a deliberate weakness in the beam is an appropriate approach for forming plastic hinges in the beam. The results of this study indicate that, while the stiffness of the structure doesn't change significantly, the vierendeel mechanism develops around the opening, leading to the formation of plastic hinges in the beam and improving the ductility of the structure.

The behavior of composite beams with web openings under negative bending is one of the topics investigated in previous studies. The primary failure mode in composite cantilever beams with web openings subjected to negative bending is often the shear failure of the concrete slab at the opening location which severely reduces the beam's load-carrying capacity [13]. Another type of beams with openings in the web is cellular beams. Extensive studies have been conducted on these beams, covering various topics such as load-carrying capacity [14], out-of-plane behavior [15], elastic-plastic analysis of cellular beams [16], and finite element analysis [17,18].

The use of stiffeners around the openings in castellated beams is an important topic. Numerous experimental studies have been carried out in this regard, and results indicate that using horizontally oriented stiffeners of larger length is the best approach to enhance the beam's load-carrying capacity and ductility [19,20]. Furthermore, studies on the behavior of castellated beams with horizontal stiffeners around openings have shown that shear failure at the opening location and flexural mechanism are the primary failure modes [21]. More recent studies have shown that the use of CFRP and mild steel stiffeners in composite castellated beams, increases the load-carrying capacity and decreases mid-span deflection [22–26]. A design approach is presented in the AISC DG31 [27] for the design of composite castellated beams. When the beam is fully composite, the force in the upper T-shape section is assumed to be zero. In this study the effect of this assumption on the load carrying capacity of composite castellated beam is investigated.

2. Flexural capacity of composite castellated beam

Design formulations for composite castellated beams are presented in AISC DG31. The shear force and moment at the center of the openings are determined and compared to the corresponding capacities according to AISC DG31 specifications. When a sufficient number of shear connectors are embedded throughout the length of the beam and full composite action is achieved, AISC DG31 assumes that the concrete slab resists all compressive stresses. Under these conditions the force in the upper T-shaped section is considered to be zero. Fig. 1 illustrates the load distribution for the cross-section under complete plasticity conditions with two assumptions: ignoring the force in the upper T-shaped section (DG31) and applying the traditional distribution. The flexural capacity is calculated for both load distribution conditions using equilibrium equations on a fully plastic section. The obtained values are subsequently compared with the results of numerical analysis.

3. Numerical modeling

3.1. Characteristics of the specimens

The geometric characteristics and dimensions of the castellated beam openings, the composite castellated beam section along with the specifications of the concrete slab, and the composite roof plan considered in this study are shown in Fig. 2 a to c respectively.
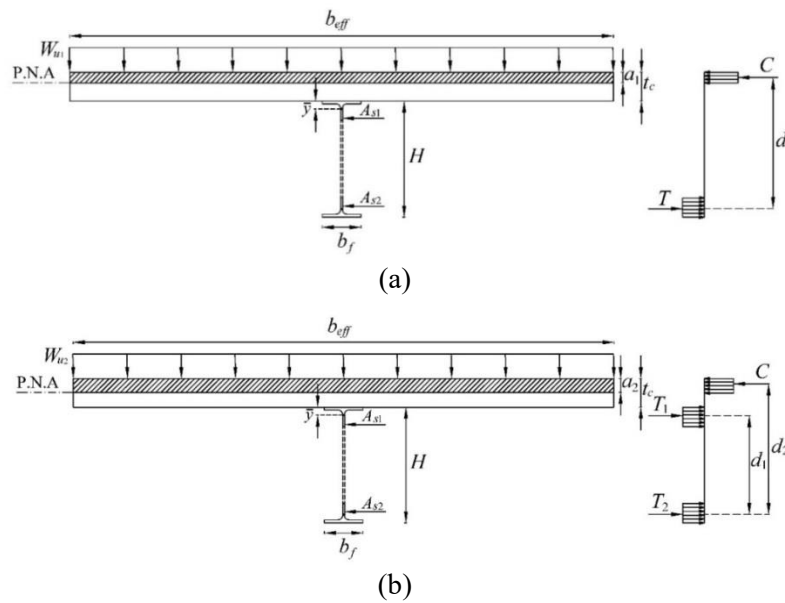
(a)

(b)

Fig. 1. Stress distribution on plastic section (a) based on AISC DG31 (b) traditional distribution.
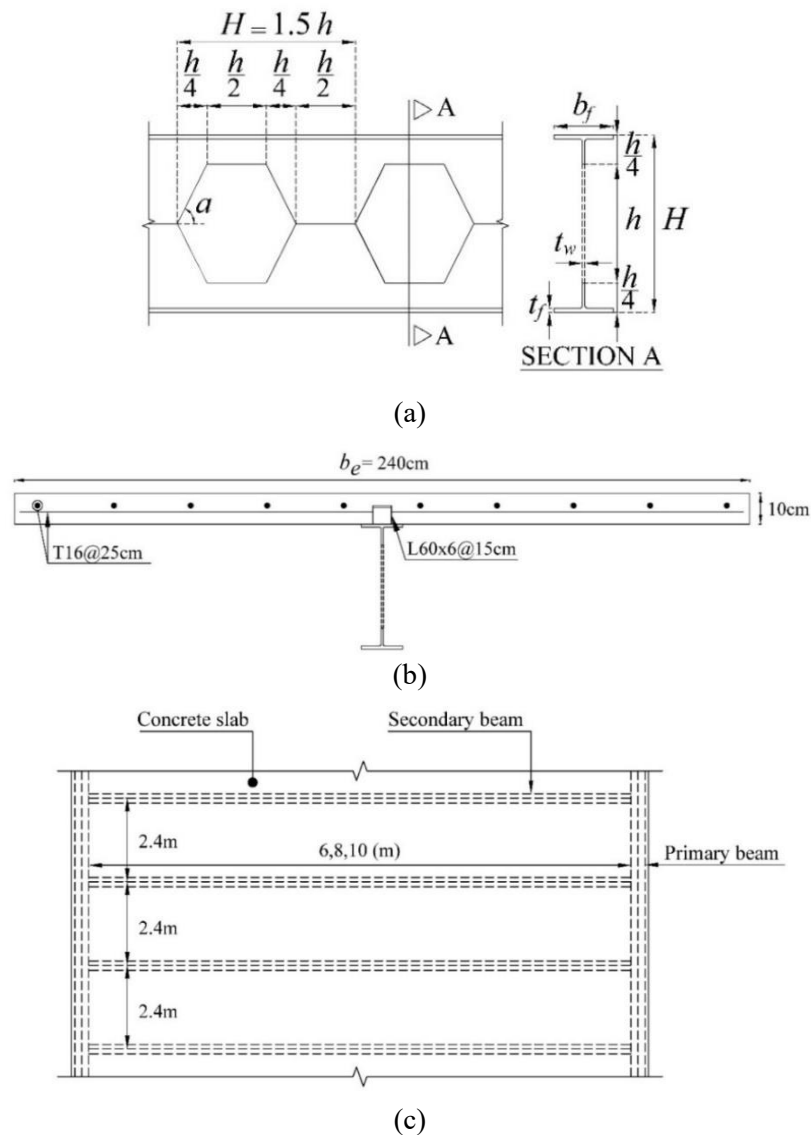

(a)

(b)

(c)

Fig. 2. Characteristics of the finite element model (a) geometry of the castellated beam (b) geometry of the composite beam (c) roof plan.

In the finite element analysis, an intermediate beam within the roof was modeled, accompanied by a concrete slab with a thickness of 10 centimeters and a width of 2.4 meters. Nine castellated beams have been modeled using standard sections such as IPE220, IPE240, and IPE270. Additionally, nine I-section steel beams with the same cross-sectional area and height as the castellated beams were modeled for spans of 6, 8, and 10 meters. Castellated beams have been investigated in two formats: one with first openings filled and the other with openings extending to the end of the beam. In most composite beams, the plastic neutral axis is within the concrete slab, and the flexural capacity is governed by the steel beam's cross-sectional area. Therefore, composite beams with the same cross-sectional area and height as castellated beams have been modeled.

The objective of modeling these beams was to investigate the impact of having consecutive holes in the web of castellated beams on their load-carrying capacity. The specimens with the name SW represent composite beams with a cross-sectional area equivalent to castellated beams. The castellated beam specimens are introduced with the name CPE. The * suffix after the names of CPE* specimens corresponds to specimens where the first openings were not filled. The modeled specimens of CPE330, CPE330*, and SW330 are shown in Fig. 3. The geometric specifications of the modeled specimens are listed in Table 1.

3.2. Finite element modeling

The behavior of composite castellated beams was investigated in this study using finite element analysis. After modeling the specimens, a nonlinear static analysis was conducted to determine the force-displacement curves and calculate the load-carrying capacity. Furthermore, the failure modes observed at the end of the analysis have been discussed.

In this analysis, three-dimensional eight-node (C3D8) solid elements are used to model concrete slab. Castellated beam, stiffeners and shear connectors are modeled using three-dimensional four-node (S4R) shell elements. In addition, reinforcement bars are modeled using three-dimensional two-node (T3D2) truss elements. The types and dimensions of these elements are provided in Table 2.

The castellated beams are first modeled as I-shaped sections, and then openings with specific dimensions are inserted along the length of the beam using cut extrude feature to form the castellated structure. The shear connectors are merged into the castellated beams, forming a unified component to facilitate load transfer and composite behavior. Considering that the investigation of the nonlinear behavior of shear connectors and the mechanism of shear transfer was not the main objective of this study, this modeling technique for achieving full composite action is acceptable.

The interaction between the concrete-reinforcement bars and concrete-shear connectors was established in a manner that constrained the translational degrees of freedom of the embedded parts in concrete. Loading of the specimens was conducted in two steps. In the first step, the specimens were subjected to service loads of 200 kgf/m^2 and 300 kgf/m^2 for dead and live loads respectively. The applied load increases linearly after the start of the second step until the beam collapses. This quasi-static loading approach allows for the development of the beam's force-displacement curve.

In this study, a composite roof's intermediate beam is modeled. Therefore, for symmetry purposes, the longitudinal edges of the concrete slab in the x-direction are constrained. Furthermore, to apply the boundary conditions of a simply supported beam, the edge of the web at both ends of the beam in the y-direction is constrained. For model stability during analysis, one point of the beam has also been constrained in all three translational directions. Fig. 4 illustrates the applied boundary conditions on the models. It should be noted that vertical stiffeners have been utilized to prevent the negative effects of stress concentration near the supports and the formation of compressive buckling.
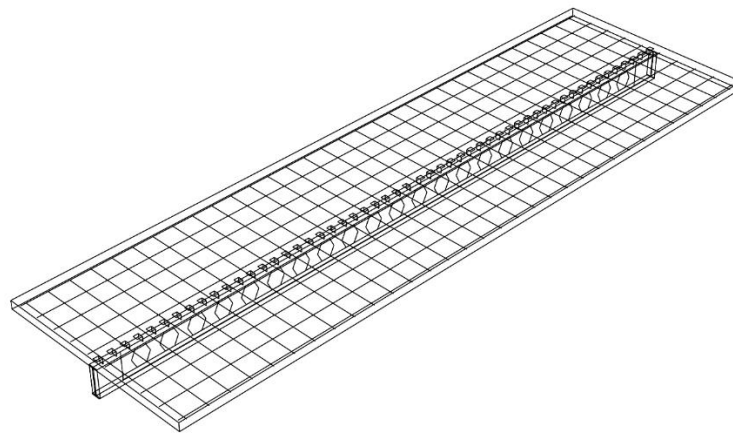
(a)
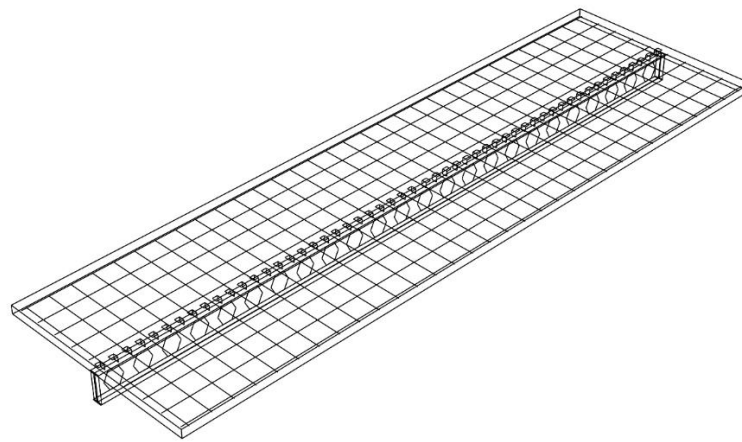
(b)
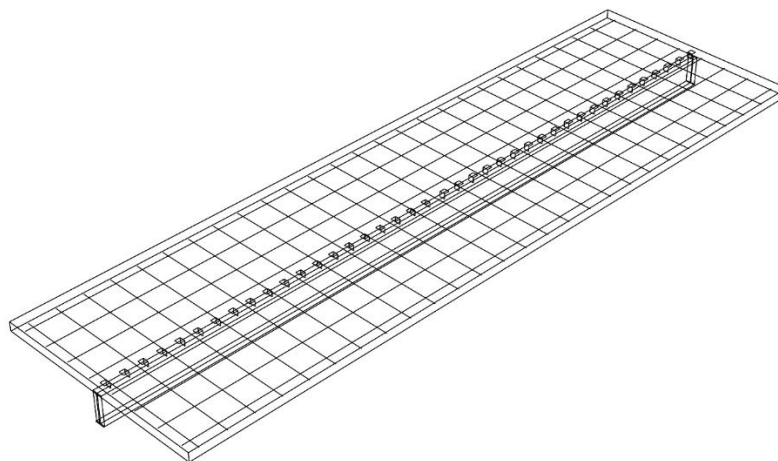
(c)

Fig. 3. FE models (a) CPE330 (b) CPE330* (c) SW330.

Table 1. Geometric specification of the specimens.

Name	H (mm)	h (mm)	b_f (mm)	t_f (mm)	t_w (mm)	a (degree)
CPE330	330	220	110	9.2	5.9	63
CPE360	360	240	120	9.8	6.2	63
CPE405	405	270	135	10.2	6.6	63
SW330	330	---	110	6.3	4.05	---
SW360	360	---	120	6.86	4.34	---
SW405	405	---	135	7.03	4.55	---

Table 2. Element types and dimensions.

Part	Element type	Mesh size (mm)
Castellated beam	S4R (Shell)	15
Shear connector	S4R (Shell)	15
Stiffener	S4R (Shell)	15
Concrete slab	C3D8R (Solid)	20
Rebar	T3D2 (Wire)	50
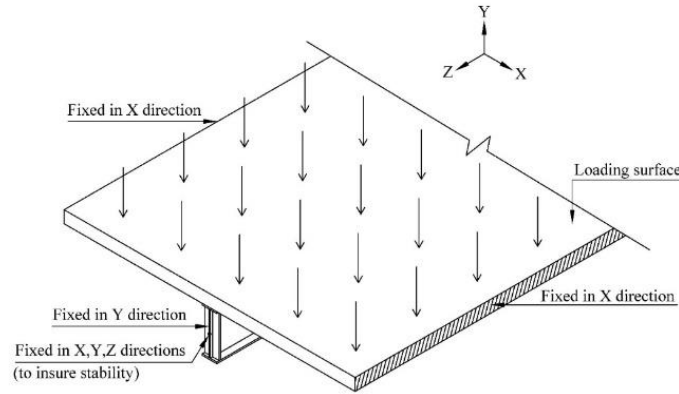
Fig. 4. Boundary conditions of the model.

3.3. Material properties

3.3.1. Concrete

Due to the occurrence of cracking, the behavior of concrete under uniaxial stress is nonlinear. Various studies have reported that the point at which nonlinear behavior in concrete begins ranges between 30% and 40% of its compressive strength. After concrete reaches its maximum strength at a strain of around 0.002, the stress-strain curve drops significantly until crushing failure occurs.

According to the ACI318-19, the elastic modulus of concrete is calculated using the following equation:

$$E_c = 0.043 w_c^{1.5} \sqrt{f_c'} \text{ (in MPa)} \tag{1}$$

In the above equation, w_c and f_c' denote the specific weight and compressive strength of concrete, respectively.

The Concrete Damage Plasticity (CDP) model has been utilized to simulate the nonlinear behavior of concrete. Plastic strains are calculated in the CDP model using the following equations:

$$\varepsilon_t^{pl} = \varepsilon_t^{ck} - \left(\frac{d_t}{1-d_t} \right)\left(\frac{\sigma_t}{E_0} \right) \text{ (in tension)} \tag{2}$$

$$\varepsilon_c^{pl} = \varepsilon_c^{in} - \left(\frac{d_c}{1-d_c} \right)\left(\frac{\sigma_c}{E_0} \right) \text{ (in compression)} \tag{3}$$

In these equation, d_c and d_t denote damage parameters in compression and tension respectively; ε_t^{ck} and ε_c^{in} are illustrated in Fig. 5. The parameters of the CDP model are presented in Table 3. In this study, the viscosity parameter of the concrete was set to a small, non-zero value to facilitate analytical convergence. The mechanical properties and stress-strain curve considered for concrete are presented in Table 4 and Fig. 6, respectively.

Table 3. CDP Parameters [28].

Parameters	Value
Dilation angle (ψ)	31°
Eccentricity (e)	0.1
Viscosity parameter (μ)	0.001
fb0/fc0	1.16
Kc	0.667

Table 4. Mechanical properties of the concrete [29].

Parameters	Value
Compression strength (MPa)	30
Modulus of elasticity (MPa)	27691
Specific weight (N/mm3)	2.4×10-5
Poisson's ratio	0.15

3.3.2. Steel

In this research, the behavior of steel materials, including castellated beams, shear connectors, rebars, and stiffeners, has been defined in a nonlinear manner. An elastic, perfectly plastic model has been employed to represent the nonlinear behavior of these steel materials. To simplify the modeling process, strain hardening has been neglected in this approach.

Figure 7 shows the stress-strain curve of the steel considered in this research. Table 5 shows the mechanical properties of steel materials.

3.4. Validation of proposed modeling technique

The method utilized for modeling composite castellated beams has been validated by comparing the results to experimental research. For this purpose, one of the composite beam specimens of Nie et al. [30] has been modeled and subjected to finite element analysis. Fig. 8 shows the characteristics of the experimental specimen.

The composite beam considered for validation has a simple connection and is subjected to concentrated loading at specified locations. The applied load increases linearly until the beam undergoes a mechanism. Fig. 9 shows displacement of the model developed from the experimental specimen using finite element modeling. Fig. 10 shows the comparison between force-displacement diagrams obtained from the finite element analysis results and the experimental data.

It can be observed that the two diagrams exhibit an acceptable level of agreement with each other, validating the modeling approach considered. It should be noted that the slight differences in the yield force may arise from the simplifications made in the modeling assumptions and material definitions.

(a)   (b)
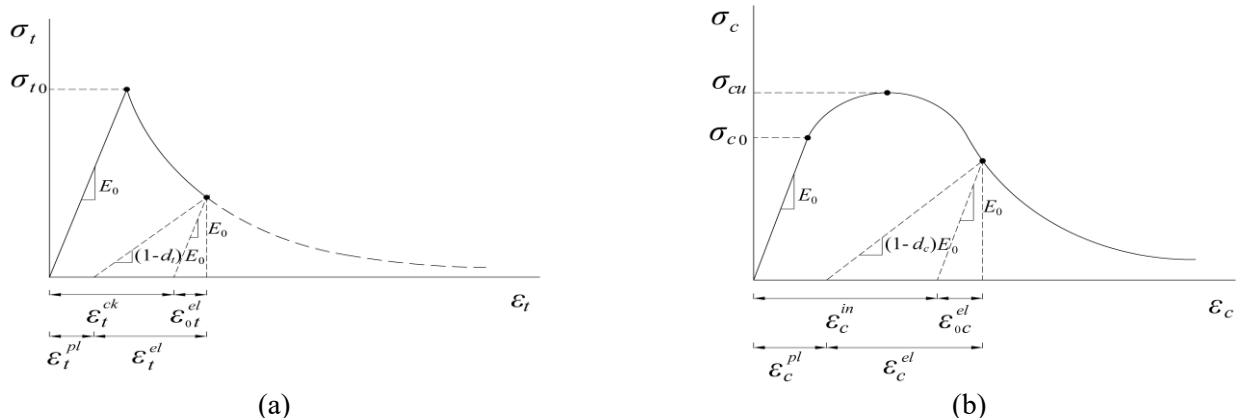
Fig. 5. Stress-strain curve of concrete for definition of unloading data (a) in tension (b) in compression [28].
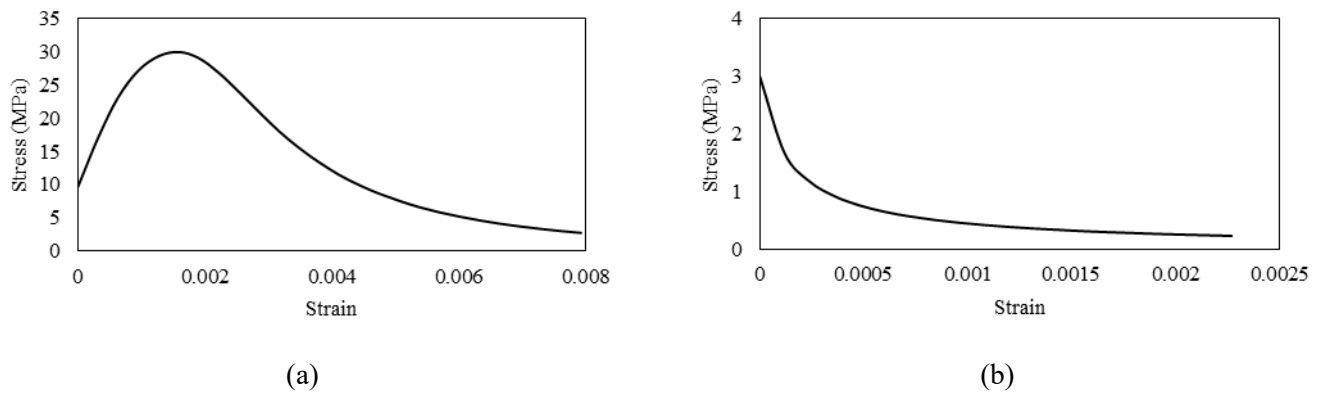
(a)   (b)

Fig. 6. Nonlinear behavior of concrete considered in analysis (a) in compression (b) in tension.
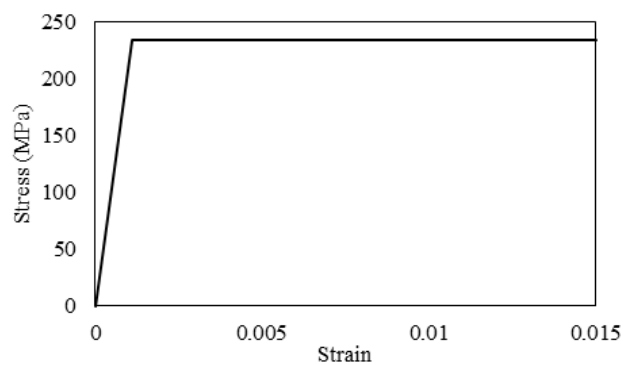

Fig. 7. Elastic, perfectly plastic model of steel materials considered in analysis.

Table 5. Mechanical properties of the steel [31].

Parameters	Value
Yield strength (MPa)	235
Modulus of elasticity (MPa)	200000
Specific weight (N/mm3)	7.85×10^{-5}
Poisson's ratio	0.3
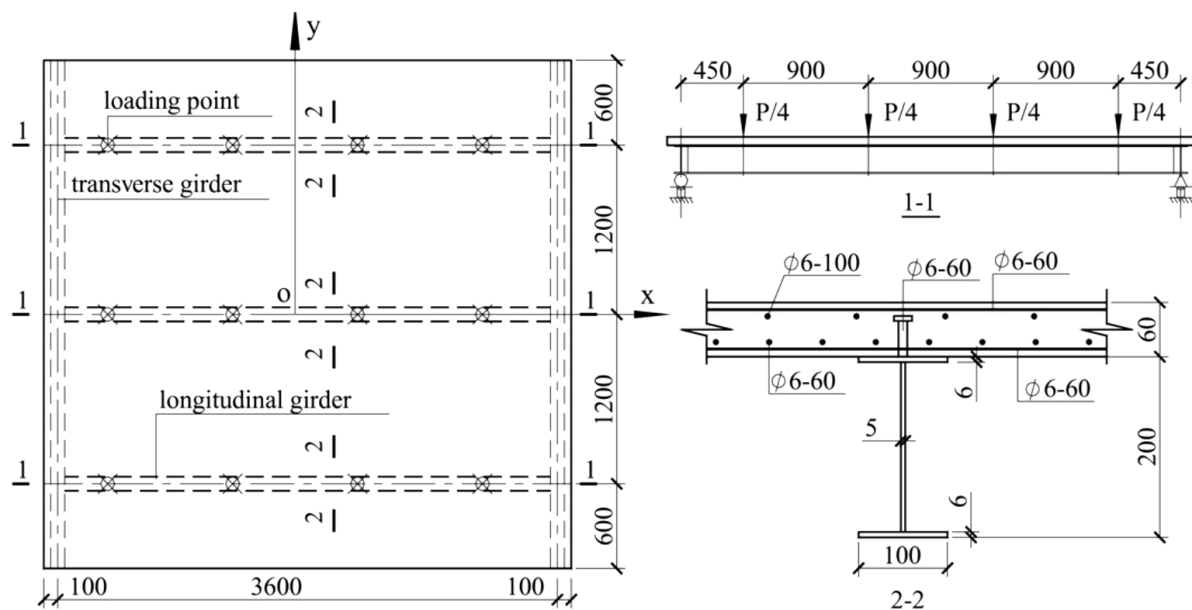
Fig. 8. Characteristics of experimental specimen [30].
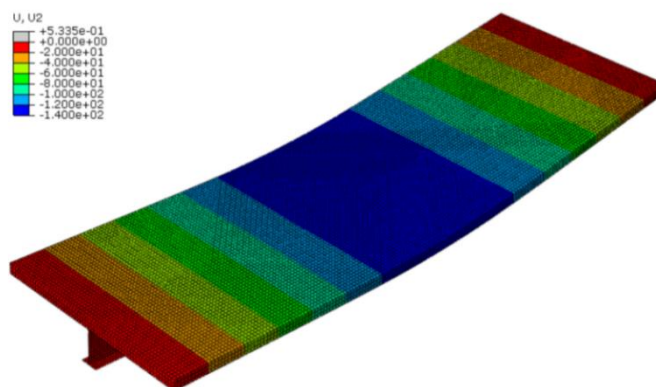
Fig. 9. Displacement of the developed FE model in Y direction.
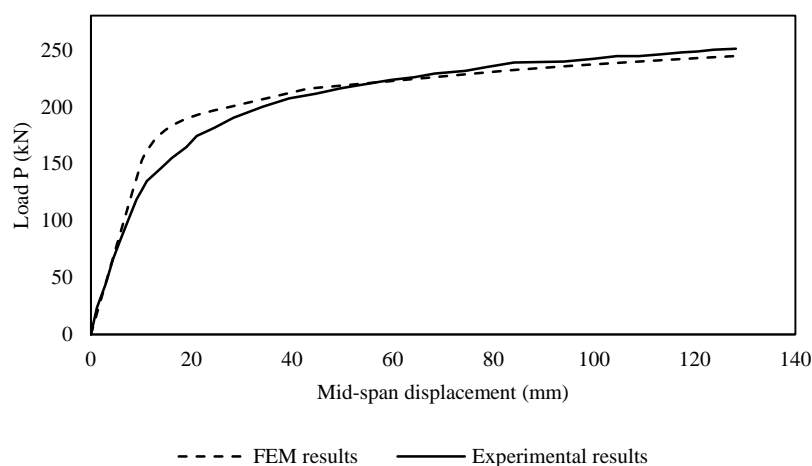
Fig. 10. Comparison between experimental [30] and FE model results.

4. Results

4.1. Failure modes

In composite castellated beams, lateral-torsional buckling does not occur due to the lateral bracing provided by the concrete slab. The primary failure modes observed in this analysis are the vierendeel mechanism and yielding of the bottom T-shaped section, which occur at the middle third of the span. Other failure modes such as local buckling, web-post buckling, and concrete slab crushing have also been observed in some of the specimens. Fig. 11 shows the Von-Mises stress of elements for two beams, CPE330 and CPE330*, in a 6-meter span. Fig. 12 shows the Von-Mises stress of elements for the CPE360 beam in spans of 6, 8, and 10 meters.
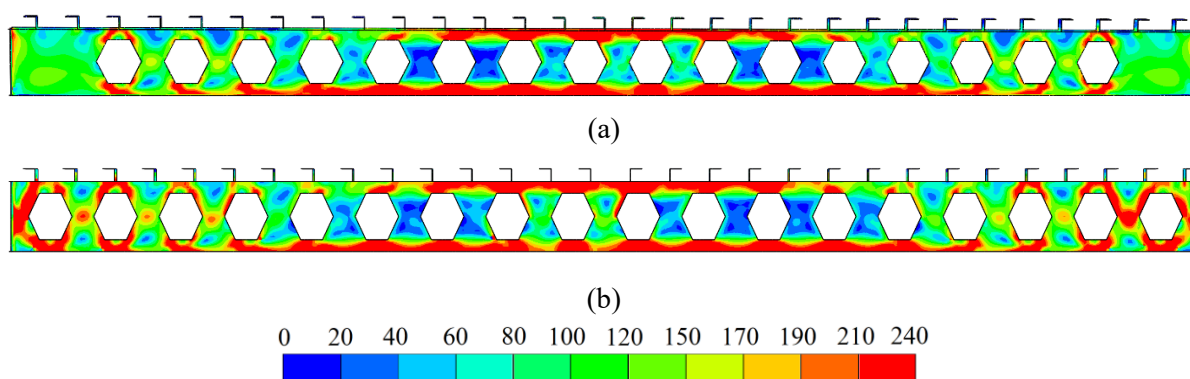

(a)

(b)

Fig. 11. Von-Mises stress distribution (MPa) (a) CPE330 (b) CPE330*.

(a)

(b)

(c)

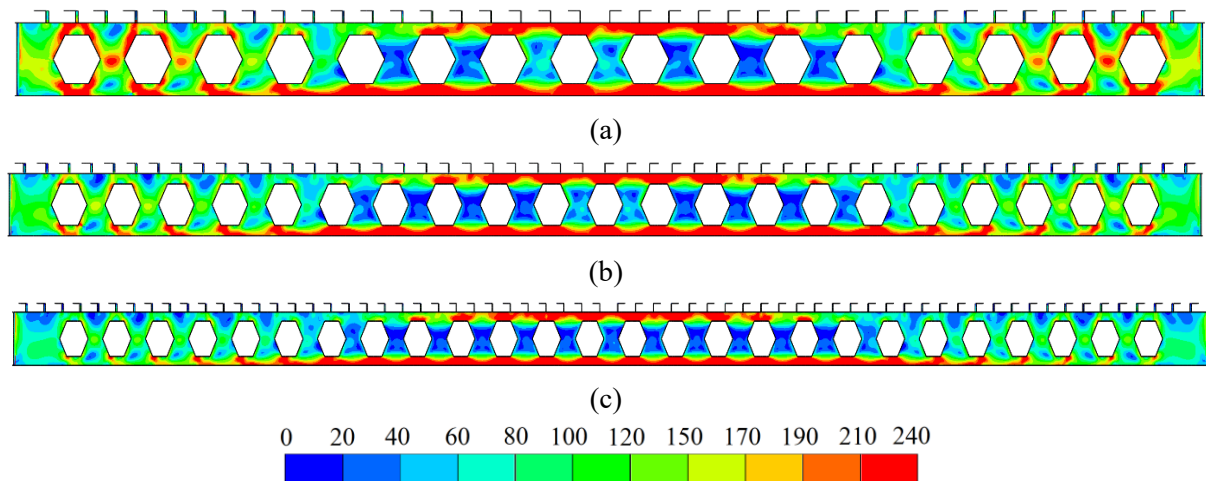0   20   40   60   80   100   120   150   170   190   210   240

Fig. 12. Von-Mises stress distribution in CPE360 (MPa) (a) 6 m (b) 8 m (c) 10 m.

## 4.2. Axial strain in concrete and plastic neutral axis

In composite beams, the plastic neutral axis is assumed to be positioned within the concrete slab. This assumption is validated using the results of finite element analysis. Fig. 13 to Fig. 15 show the axial strain in concrete at slab height for specimens CPE330, CPE360, and CPE405 respectively. The position of the plastic neutral axis corresponds to the point where the axial strain becomes zero.
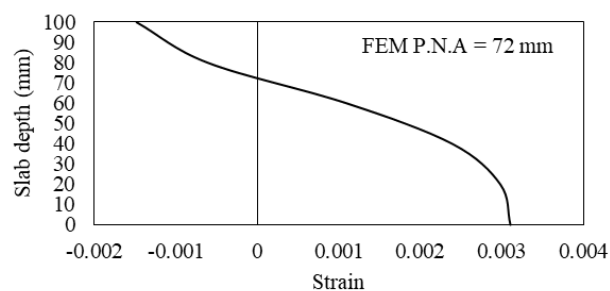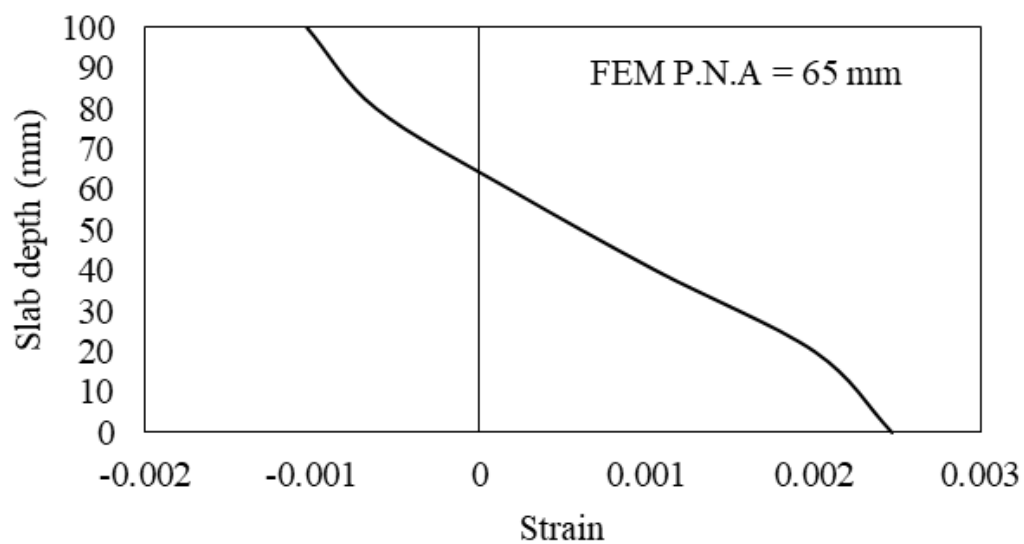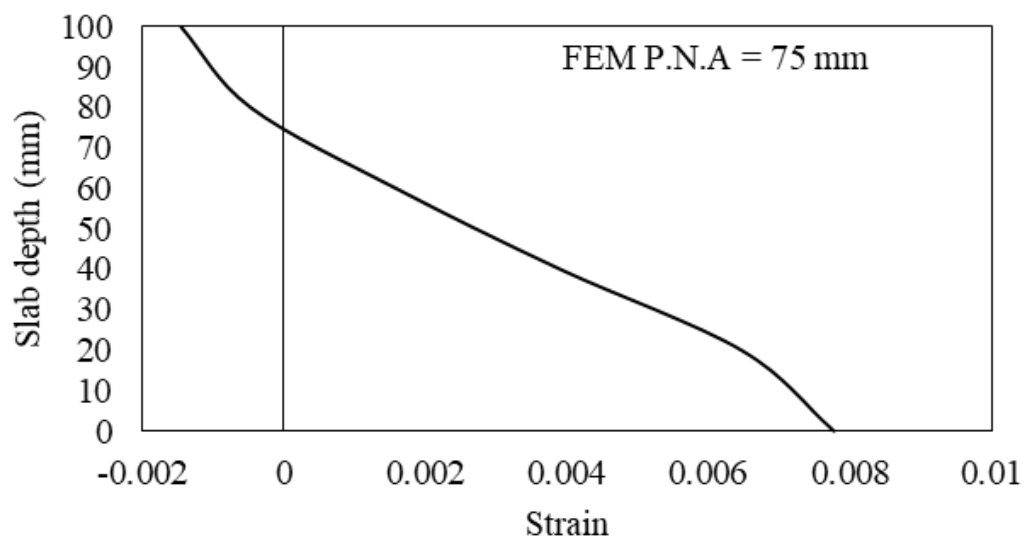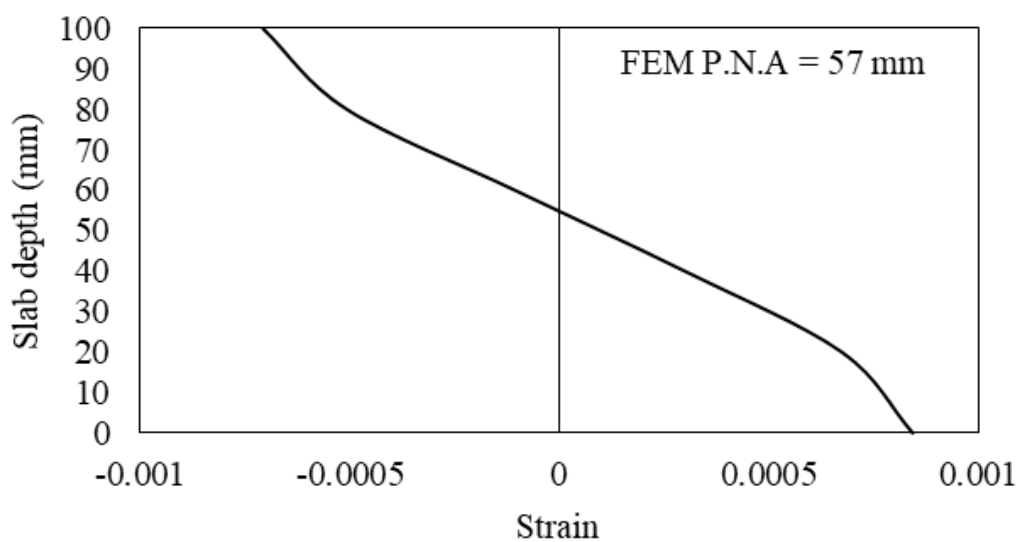

(a)
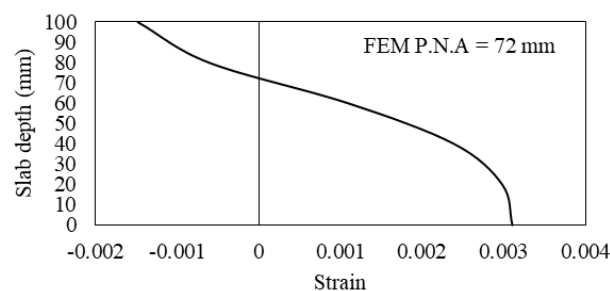
(b)
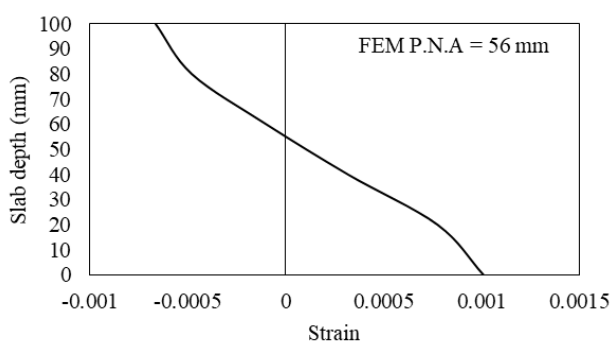
(c)

Fig. 13. Axial strain of concrete in CPE330 (a) 6 m (b) 8 m (c) 10 m.
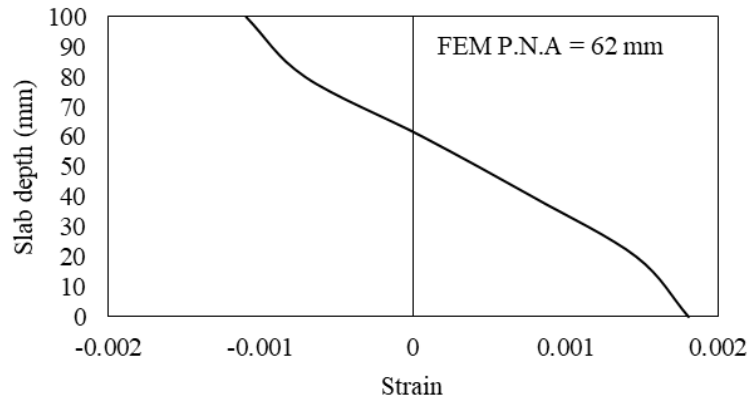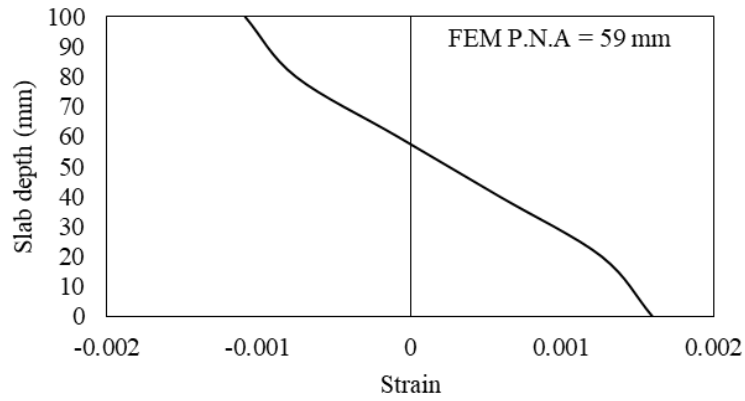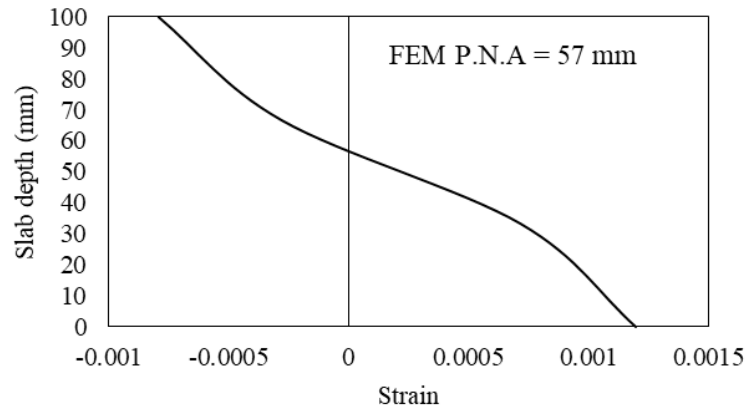
(a)

(b)

(c)

Fig. 14. Axial strain of concrete in CPE360 (a) 6 m (b) 8 m (c) 10 m.

(a)

(b)

(c)

Fig. 15. Axial strain of concrete in CPE405 (a) 6 m (b) 8 m (c) 10 m.

4.3. Load-carrying capacity

The load-carrying capacity of the beams has been calculated based on finite element analysis results and force-displacement diagrams. Furthermore, using the principles of plastic analysis presented in section 2 and by developing plastic equilibrium equations, the load-carrying capacity of the beams can be calculated for the two mentioned load distributions. Fig. 16 to Fig. 18 show force-displacement diagrams derived from finite element analysis results. Tables 6 to 8 present the calculated load-carrying capacity for the specimens. In these tables, the load-carrying capacity obtained from finite element analysis, the load-carrying capacity calculated assuming AISC DG31 load distribution and the load-carrying capacity calculated assuming traditional load distribution are denoted by $P_{u\text{-}FEM}$, $P_{u\text{-}DG}$ and $P_{u\text{-}TD}$, respectively.
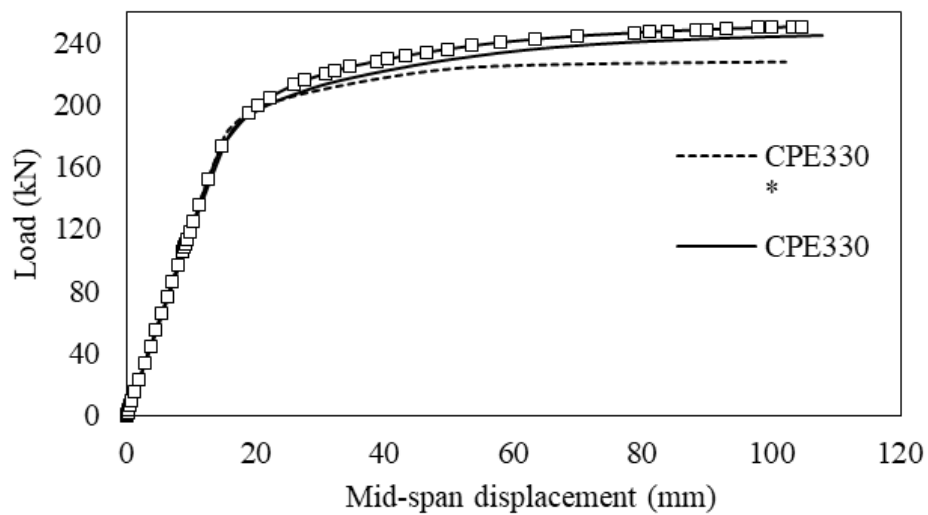
(a)
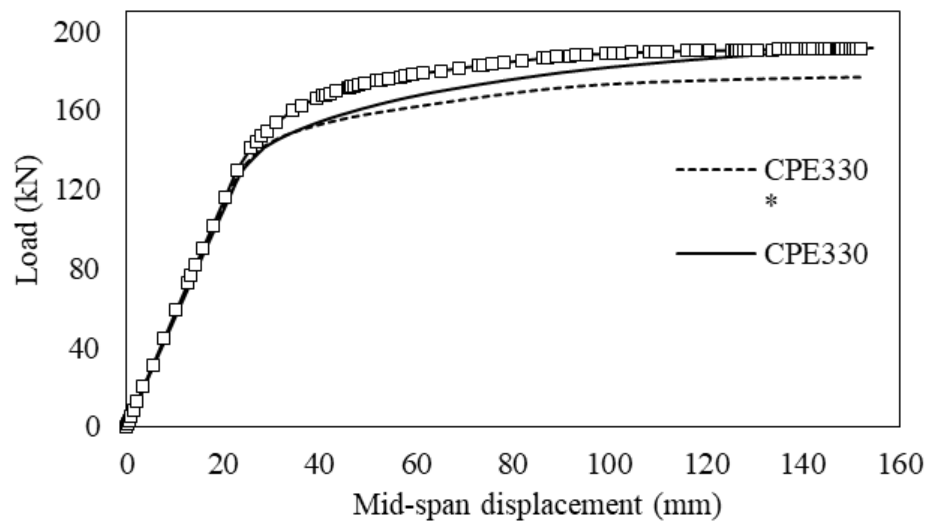
(b)
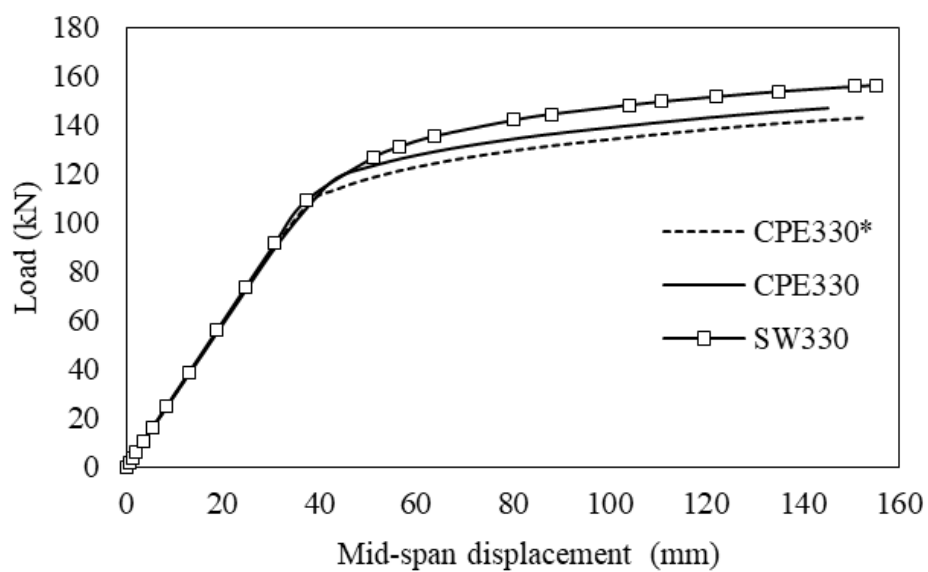
(c)

Fig. 16. Load-displacement diagram for CPE330, CPE330*, SW330 (a) 6 m (b) 8 m (c) 10 m.

14

(a)

(b)

(c)

Fig. 17. Load-displacement diagram for CPE360, CPE360*, SW360 (a) 6 m (b) 8 m (c) 10 m.
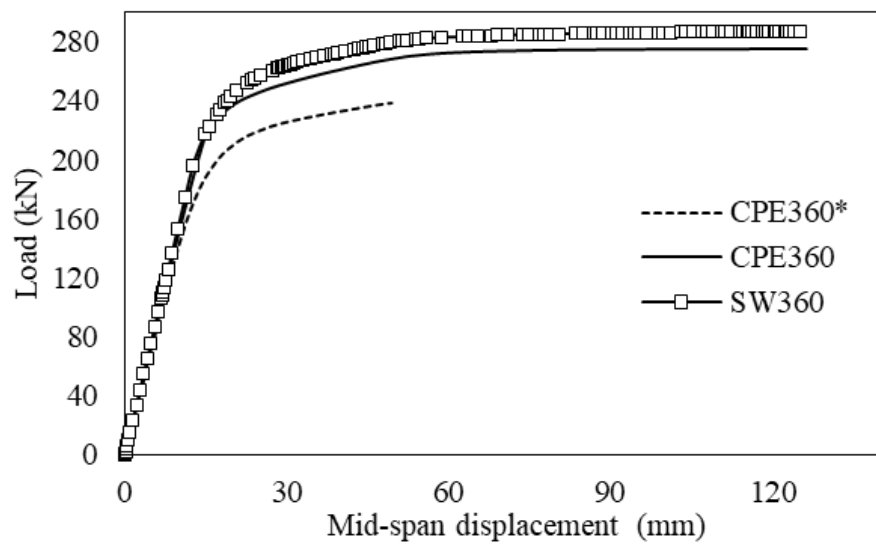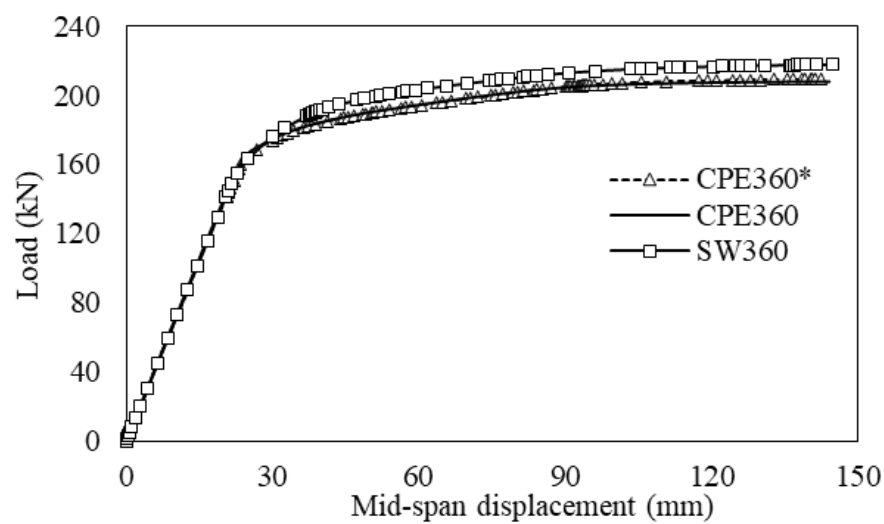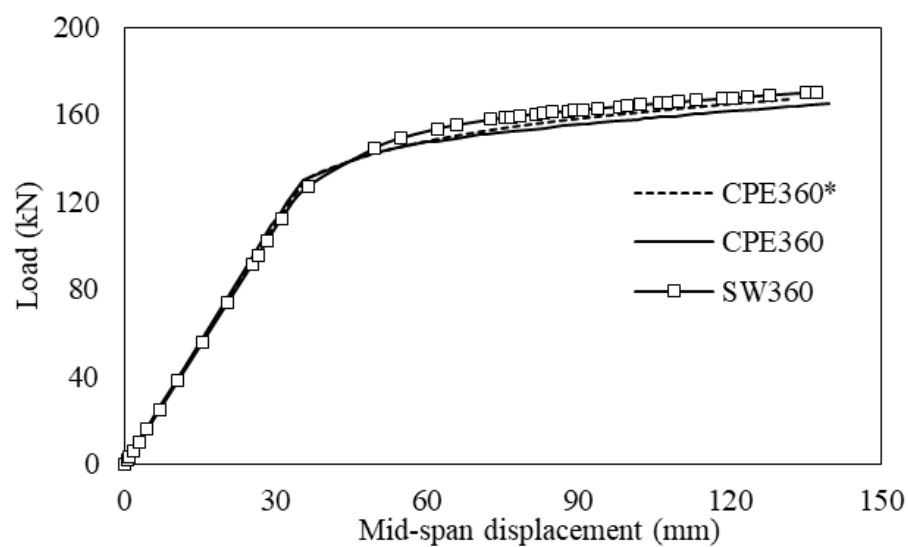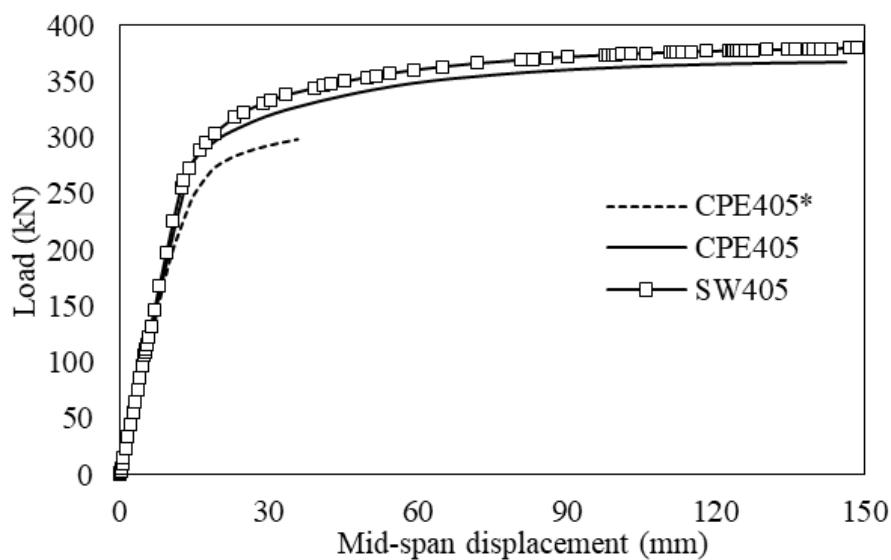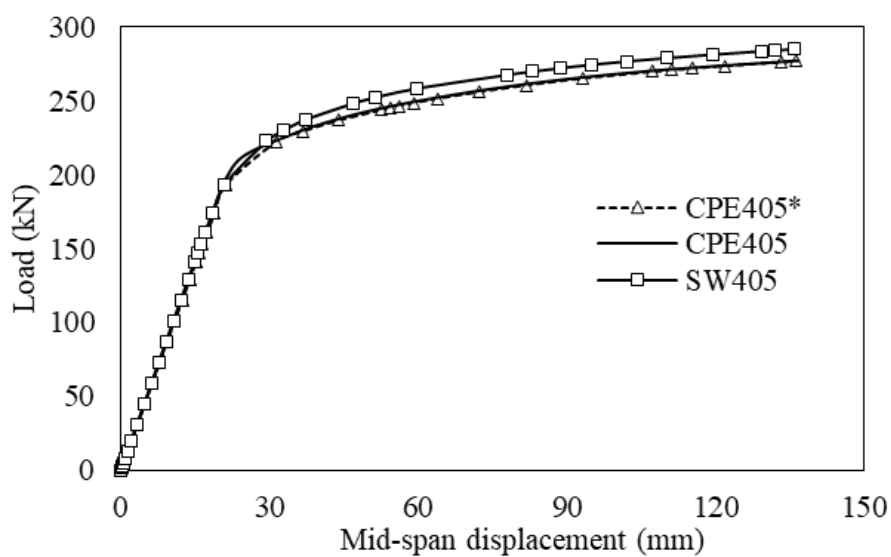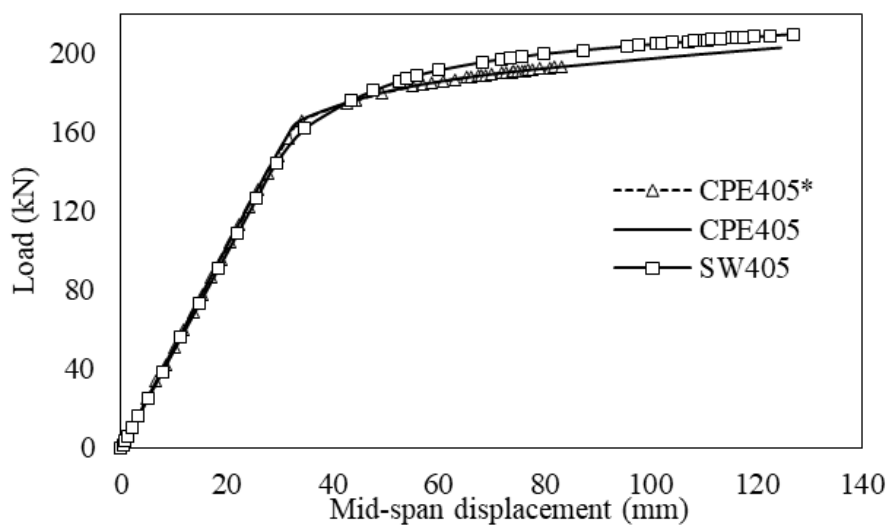
(a)

(b)

(c)

Fig. 18. Load-displacement diagram for CPE405, CPE405*, SW405 (a) 6 m (b) 8 m (c) 10 m.

Table 6. Load-carrying capacity of the specimens: $P_{u\text{-}FEM}$.

Specimen	$P_{u\text{-}FEM}$ (kN)		
	L = 6 m	L = 8 m	L = 10 m
CPE330	244	191	150
CPE330*	227	176	143
SW330	250	191	155
CPE360	275	208	165
CPE360*	238	208	167
SW360	287	218	170
CPE405	367	277	205
CPE405*	298	277	193
SW405	380	285	210

Table 7. Load-carrying capacity of the specimens: $P_{u\text{-}TD}$.

Specimen	$P_{u\text{-}TD}$ (kN)		
	L = 6 m	L = 8 m	L = 10 m
CPE330, CPE330* SW330	219	164	131
CPE360, CPE360* SW360	272	204	163
CPE405, CPE405* SW405	342	257	205

Table 8. Load-carrying capacity of the specimens: $P_{u\text{-}DG}$.

Specimen	$P_{u\text{-}DG}$ (kN)		
	L = 6 m	L = 8 m	L = 10 m
CPE330, CPE330* SW330	175	132	105
CPE360, CPE360* SW360	220	166	133
CPE405, CPE405* SW405	282	212	170

5. Discussion

5.1. Discussion on failure modes

The yielding status of the elements and therefore the failure modes formed in all specimens have been identified by comparing the Von-Mises stress values with the yield stress of steel. The findings indicate that the bottom T-shaped section yields in all specimens within the middle third of the span. Additionally, most specimens exhibit failure modes such as the vierendeel mechanism, local buckling, web-post buckling, and local yielding of the shear connectors. Some local failure modes in castellated beams, such as weld-joint rupture, are not detectable in this analysis due to modeling limitations.

Since shear force is maximum near the supports, it can be seen that filling the span's first openings delays the start of the vierendeel mechanism. Furthermore, in specimens with a 10-meter span when the first openings are filled, the vierendeel mechanism is not among the observed failure modes.

By reviewing the analysis results, it is discovered that the higher section height and short span of the beam correspond to the higher possibility of the vierendeel mechanism. In addition, in the case of long span beams and short section height, a flexural mechanism at the middle third of the span is the primary failure mode. In cases where the distance between the first opening and the support is small, it is observed that the initiation of local yielding at the first web-post occurs earlier than expected, leading to premature failure and a sudden drop in the force-displacement curve of the beam. This results in the beam not reaching its expected load-carrying capacity. Therefore, it is recommended to ensure an appropriate distance between the first opening and the support to avoid such failure. In the case of castellated beams, to prevent local failures, it is recommended to fill the first openings of the span.

5.2. Discussion on plastic neutral axis

For most cases in composite beams, the assumption in Section 2 that the plastic neutral axis lies within the concrete and that all compressive forces are resisted by the concrete while all tensile forces are resisted by the steel section is generally valid.

The axial strain in concrete at slab height has been plotted for all specimens to verify the validity of this assumption. Considering that the axial strain in the plastic neutral axis is zero, the depth of the concrete slab where the strain is zero indicates the location of the plastic neutral axis. The plastic neutral axis lies within the concrete slab in all specimens, as indicated by the plotted diagrams, confirming the validity of the premise. As a result, in the calculations of the composite section's flexural capacity, the concrete section resists all compressive forces whereas the steel section resists all tensile forces.

5.3. Discussion on load carrying capacity

After performing finite element analysis and extracting results, force-displacement diagrams of the specimens have been plotted. The percentage change in the obtained load-carrying capacities is illustrated in Fig. 19. In this diagram, the terms SW/CPE and SW/CPE* denote the percent change in load-carrying capacity between castellated beams and solid-web beams, and the percentage change in load-carrying capacity between castellated beams with unfilled openings and solid-web beams, respectively. Furthermore, the terms TD/CPE and DG/CPE represent the percentage change in load-carrying capacity calculated assuming a traditional load distribution and the load-carrying capacity obtained from finite element analysis, and the percentage change in load-carrying capacity calculated assuming AISC DG31 load distribution and the load-carrying capacity obtained from finite element analysis, respectively.
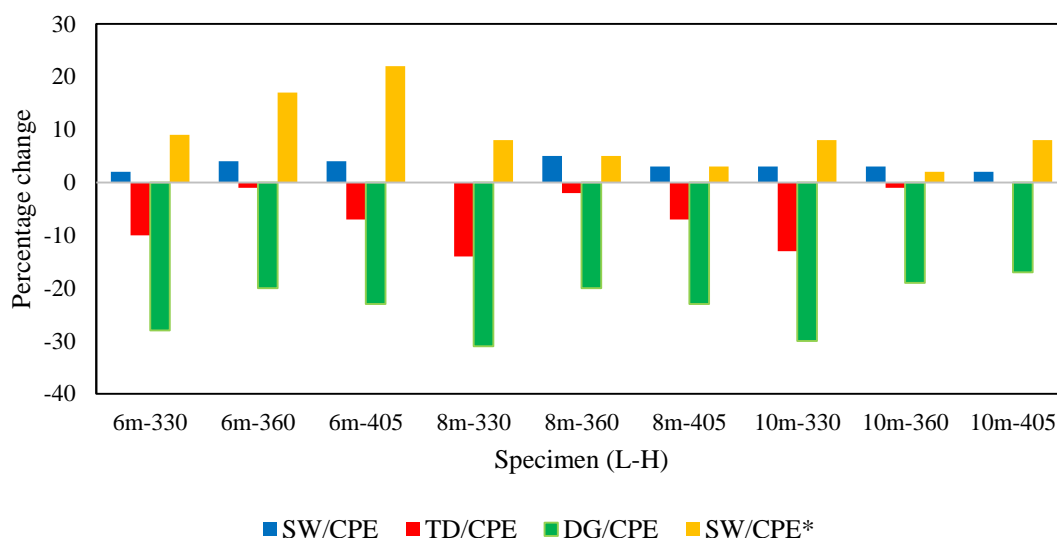
Fig. 19. Percentage change of load carrying capacities for all specimens.

The force-displacement diagrams show similar elastic behavior across all three beam types. Solid-web beams (SW) have on average 5% higher load-carrying capacity than castellated beams (CPE). The plastic neutral axis is within the concrete in all the specimens, and the flexural capacity corresponds to the beam's cross-sectional area. Given that the cross-sectional areas of the SW and CPE specimens are equal, the observed drop in capacity could be related to the existence of web openings. This capacity loss is on average 10% for CPE* specimens with unfilled first openings. In the case where local yielding has occurred in the web-post due to the proximity of the first opening to the support and the beam cannot achieve its capacity, the load-carrying capacity of the specimens has been decreased by a maximum of 22%. As a result, it is recommended that the first opening of the castellated beams be filled.

The load-carrying capacity calculated using plastic equilibrium and traditional load distribution ($P_{u\text{-}TD}$) is 6% lower on average than the values obtained from finite element analysis results. This decrease in capacity is most significant in beams with a height of 330 millimeters, reaching a maximum of 14%. The load-carrying capacity calculated using plastic equilibrium and the AISC DG31 load distribution ($P_{u\text{-}DG}$) is 24% lower on average than the values obtained from finite element analysis. This decrease in capacity is most significant in beams with a height of 330 millimeters, reaching a maximum of 31%.

According to the finite element analysis results, the presence of openings within the web has little impact on the load-carrying capacity of castellated beams. Furthermore, the utilization of vertical stiffeners at stress concentration locations (e.g., near supports or under concentrated loads) and horizontal stiffeners around openings can prevent local failures and allow the beam to reach its maximum capacity. In this case, the utilization of composite castellated beams, especially in large-span structures, can greatly improve the project's economic efficiency. Furthermore, if the entire steel cross-section is assumed to be subjected to tensile forces, the flexural capacity and, as a result, the load-carrying capacity obtained are very close to the results of finite element analysis.

6. Conclusion

In this study, finite element analysis was performed on composite castellated beams and composite beams with the same cross-sectional area and height as the castellated beam specimens to investigate the effect of web openings on the load-carrying capacity and behavior of these beams. Furthermore, load-carrying capacities obtained from analysis results and calculated using plastic equilibrium equations were compared. Based on the study's discussions and results, these conclusions can be summarized:

- Finite element analysis has shown that in composite castellated beams, flexural mechanism occurs at the bottom T-shape section in the middle third of the span, and vierendeel mechanism can potentially form around the first openings in the web. Furthermore, if the first opening in the castellated beam is close to the support, due to the stress concentration caused by high shear force, the first web-post may experience local buckling, resulting in a significant reduction in load-carrying capacity.

- The Von-Mises stress distribution of the specimens has shown that a shorter span and a larger section height of the beam increase the probability of the vierendeel mechanism as the primary failure mode. Additionally, the distribution of axial stresses in the castellated beam has shown that over most of the beam's length, the entire steel section is subjected to tensile forces. Therefore, assuming a traditional load distribution in plastic equilibrium equations for calculating flexural capacity is applicable.

- The plastic neutral axis is assumed to be within the concrete slab in the load distribution in the composite beam, and all compressive forces are resisted by the concrete. When the axial strain of the concrete within the depth of the slab is plotted for all specimens, the axial strain within the depth of the slab becomes zero.

- The calculated load-carrying capacity corresponds reasonably well with the finite element analysis results, with an average difference of 6% when assuming a traditional load distribution. When the load-carrying capacity is calculated without considering the force in the upper T-shape section, the average difference with the finite element analysis results is 24%, showing a considerable drop in load-carrying capacity.

- The results of finite element analysis for SW, CPE, and CPE* specimens demonstrate that the load-carrying capacity of castellated beam specimens is 5% lower on average than the load-carrying

capacity of solid-web specimens. The difference increases to an average of 10% for castellated beams with unfilled first openings. The load-carrying capacity of some CPE* specimens especially with short distances between the first opening and the support is reduced by 22%. Based on the results, it can be stated that when a sufficient distance between the start of the openings and the support is considered in castellated beams, the presence of these openings has a minor impact on reducing the load-carrying capacity of the beam when compared to solid-web beams.

It should be noted that the results and conclusions reported in this study are based on numerical analysis performed with finite element analysis. Further research on this topic, as well as experimental research, could be the next step in supporting the results of this study. A more thorough investigation into localized failure modes such as web-post buckling and weld-joint rupture as well as investigating the shear transfer mechanisms at shear connectors could also be useful research topics.

Funding

Conflicts of interest

The authors declare that they have no known competing financial interests or personal relationships that could have appeared to influence the work reported in this paper.

Authors contribution statement

Mohammad Sadeghi: Data curation; Formal analysis; Investigation; Software; Writing – original draft; Writing – review & editing.

Ehsan Dehghani: Conceptualization; Methodology; Project administration; Resources Writing – review & editing.

Mohammad Ali Fathali: Resources; Writing – review & editing.

References

[1]   Samadhan G. Morkhade, Laxmikant M. Gupta. Behavior of Castellated Steel Beams: State of the Art Review. Electron J Struct Eng 2019;19:39–48. https://doi.org/10.56748/ejse.19234.

[2]   Altifillisch MD, Cooke BR, Toprac AA. An investigation of open web expanded beams. Weld Res 1957;22.

[3]   Gardner NJ. An investigation into the deflection behavior of castellated beams. Trans Eng Inst Canada 1969;9:56.

[4]   Gibson JE, Jenkins WM. An investigation of the stresses and deflections in castellated beams. Struct Eng 1957;35:467–79.

[5]   Kerdal D, Nethercot DA. Failure modes for castellated beams. J Constr Steel Res 1984;4:295–315.

[6]   Redwood R, Cho SH. Design of steel and composite beams with web openings. J Constr Steel Res 1993;25:23–41.

[7]   Eurocode 4: Design of composite steel and concrete structures - Part 1-1: General rules and rules for buildings 2004;EN 1994-1-.

[8]   Chung K., Lawson R. Simplified design of composite beams with large web openings to Eurocode 4. J Constr Steel Res 2001;57:135–64. https://doi.org/10.1016/S0143-974X(00)00011-0.

[9]   Wang AJ, Chung KF. Advanced finite element modelling of perforated composite beams with flexible shear connectors. Eng Struct 2008;30:2724–38. https://doi.org/10.1016/j.engstruct.2008.03.001.

[10] Yang Q, Li B, Yang N. A seismic behaviors of steel moment resisting frames with opening in beam web. J Constr Steel Res 2009;65:1323–36. https://doi.org/10.1016/j.jcsr.2009.01.007.

[11] Sakr MA, Sakla SSS. Long-term deflection of cracked composite beams with nonlinear partial shear interaction: I - Finite element modeling. J Constr Steel Res 2008;64:1446–55. https://doi.org/10.1016/j.jcsr.2008.01.003.

[12] Tahmasebinia F, Ranzi G. Three-Dimensional FE Modelling of Simply-Supported and Continuous Composite Steel-Concrete Beams. Procedia Eng 2011;14:434–41. https://doi.org/10.1016/j.proeng.2011.07.054.

[13] Chen T, Gu X, Li H. Behavior of steel-concrete composite cantilever beams with web openings under negative moment. Int J Steel Struct 2011;11:39–49. https://doi.org/10.1007/S13296-011-1004-8.

[14] Erdal F, Saka MP. Ultimate load carrying capacity of optimally designed steel cellular beams. J Constr Steel Res 2013;80:355–68. https://doi.org/10.1016/j.jcsr.2012.10.007.

[15] Nseir J, Lo M, Sonck D, Somja H, Vassart O, Boissonnade N. Lateral torsional buckling of cellular steel beams. Proc. Annu. Stab. Conf. Struct. Stab. Res. Counc., 2012, p. 18–21.

[16] Lawson RM, Saverirajan AHA. Simplified elasto-plastic analysis of composite beams and cellular beams to Eurocode 4. J Constr Steel Res 2011;67:1426–34. https://doi.org/10.1016/j.jcsr.2011.03.016.

[17] Gizejowski MA, Salah WA. Numerical Modeling of Composite Castellated Beams. Compos. Constr. Steel Concr. VI, Reston, VA: American Society of Civil Engineers; 2011, p. 554–65. https://doi.org/10.1061/41142(396)45.

[18] Sweedan AMI. Elastic lateral stability of I-shaped cellular steel beams. J Constr Steel Res 2011;67:151–63. https://doi.org/10.1016/j.jcsr.2010.08.009.

[19] E.S.Ismail R, Fahmy AS, M. Tawfik N. Ultimate Behavior of Composite Castellated Beams under Vertical Loads. Int J Comput Appl 2014;108:40–6. https://doi.org/10.5120/18911-0214.

[20] Al-Dafafea T, Durif S, Bouchaïr A, Fournely E. Experimental study of beams with stiffened large web openings. J Constr Steel Res 2019;154:149–60. https://doi.org/10.1016/j.jcsr.2018.11.026.

[21] Du H, Hu X, Shi D, Fang B. Effect of reinforcement on the strength of the web opening in steel-concrete composite beam. Eng Struct 2021;235:112038. https://doi.org/10.1016/j.engstruct.2021.112038.

[22] Akrami V, Adili A, Shakeri K, Shahbazi N. An Investigation on the Cyclic Behavior of I-Shaped Beam to Circular Column Moment Connections with Channel Link. Civ Infrastruct Res 2023;9:141–61. https://doi.org/10.22091/cer.2023.9497.1485.

[23] Mali SS, Kumbhar PD. Comparative study on behaviour of castellated beams with diamond- and hexagonal-shaped openings using CFRP stiffeners. Asian J Civ Eng 2024;25:939–52. https://doi.org/10.1007/s42107-023-00823-x.

[24] Patil SS, Kumbhar PD, Kurlapkar RR. Comparative study on behavior of castellated beams of different shaped openings provided with mild steel and FRP stiffeners. Asian J Civ Eng 2024;25:1659–70. https://doi.org/10.1007/s42107-023-00869-x.

[25] Jadhav SD, Kumbhar PD. Non-linear behavior of castellated beams consisting hexagonal and diamond openings using CFRP stiffeners. Asian J Civ Eng 2024;25:4713–24. https://doi.org/10.1007/s42107-024-01075-z.

[26] Kumbhar PD, Jamadar AM. Comparative study on load carrying capacities of castellated beams provided with mild steel and CFRP stiffeners. Mater Today Proc 2023. https://doi.org/10.1016/j.matpr.2023.03.391.

[27] Fares S, Coulson J, Dinehart D. Castellated and cellular beam design. Am Inst Steel Constr 2016.

[28] Hafezolghorani M, Hejazi F, Vaghei R, Jaafar MS Bin, Karimzade K. Simplified Damage Plasticity Model for Concrete. Struct Eng Int 2017;27:68–78. https://doi.org/10.2749/101686616X1081.

[29] Committee A. Building code requirements for structural concrete (ACI 318-05) and commentary (ACI 318R-05). Am Concr Institute, Farmingt Hills, Mich 2019.

[30] Nie J-G, Tian C-Y, Cai CS. Effective width of steel–concrete composite beam at ultimate strength state. Eng Struct 2008;30:1396–407. https://doi.org/10.1016/j.engstruct.2007.07.027.

[31] Construction AI of S. Specification for structural steel buildings. ANSI/AISC 2005;36010.